RICE UNIVERSITY

Studying the Impact of RO Membrane Surface Functionalities on Alginate Fouling in Seawater Desalination

by

Jinjian Wu

A THESIS SUBMITTED
IN PARTIAL FULFILLMENT OF THE
REQUIREMENTS FOR THE DEGREE

Master of Science

APPROVED, THESIS COMMITTEE:

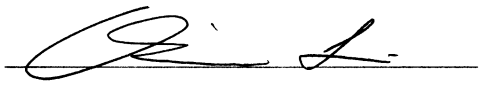

Qilin Li, Assistant Professor, Civil & Environmental Engineering

Pedro J. Alvarez, George R. Brown Professor, Department Chair, Civil & Environmental Engineering

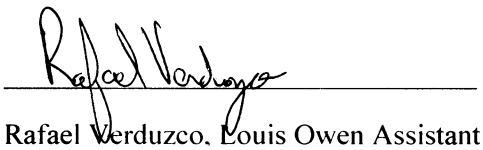

Rafael Verduzco, Louis Owen Assistant Professor, Louis Owen Junior Faculty Chair, Chemical & Biomolecular Engineering

HOUSTON, TEXAS
JULY 2011

Abstract

Studying the Impact of RO Membrane Surface Functionalities on Alginate Fouling in Seawater Desalination

by

Jinjian Wu

The objective of this research was to elucidate how specific membrane surface functionalities affect fouling by alginate in seawater desalination. Alginate adsorption on self-assembled mono-layers with –COOH, $–NH_2$, $–CONH_2$ groups under different solution conditions was studied using quartz crystal microbalance with dissipation monitoring. Cross-flow filtration experiments were performed using four commercial RO membranes to study the correlation of alginate fouling to membrane surface properties. Experimental results revealed the importance of solution condition, but surface functionality did not have significant impact on alginate adsorption equilibrium. The initial adsorption/deposition rate on the –COOH surface was the highest, while adsorption on the $–NH_2$ surface was most difficult to remove by surfactant cleaning. Filtration experiments showed that alginate fouling was more closely related to surface roughness than surface chemistry. The results suggest that surface chemistry is not an important factor for short term membrane fouling in seawater RO processes.

Acknowledgements

First of all, I would like to express my sincere gratitude to Dr. Qilin Li for her guidance and advisory during my master's study at Rice University. As my academic advisor, she introduced me to the field of my current study, guided me through various problems, and helped me achieve what I have accomplished in my research. She inspired and influenced me with her unique insight and strong self-discipline in academic studies.

The research group has been an extraordinary environment in which I have gained great supports and friendships. I would like to thank Alison Contreras for her enormous help in my study and research. I thank my fellow lab mates and friends Xiaolei Qu and Cong Yu. My hardest times were a lot easier with their company and supports. I would also like to thank the past and present group members whom I have had the honor to work with, Sen Wang, Michael Liga, Jianwei Ma and Dr. Yusik Hwang. Their passion and scientific spirit greatly inspired me.

I thank all the professors and teachers at Rice University whom I had the honor to study with. They expanded my knowledge and horizon. I would also like to thank all of my committee members, Dr. Qilin Li, Dr. Pedro Alvarez and Dr. Rafael Verduzco for their supports and guidance, especially Dr. Verduzco who generously agreed to help in my time of needs. I am also very grateful to everyone who had helped during my master thesis study, including Kun Ma from Chemical Engineering, Denise Benoit from Chemistry and Liang Gand from Rice SEA.

Last but not least, I would like to thank all my family and friends. Thank my parents for their firm belief in me, and my girlfriend for giving me courage,

TABLE OF CONTENTS

LIST OF FIGURES

LIST OF TABLES

LIST OF EQUATIONS

1, Introduction and Research Objectives

Water supply is now facing more and more severe challenges world-wide. On one hand, the global water demand has been and will keep soaring at an astonishing speed, due to the steady growth of population as well as industries. For the past sixty years, our global population has been increasing at a rate above 1.0% per year, with only the past twenty years lower than 1.5% per year [1]. During the time of 1900 to 1995, the world population increased by three times, while the fresh water demand increased six-fold [2]. Along with the need for human consumption, the world-wide rapid industrialization also boosted the need for water supply. While the industrialization and urbanization are taking place, the awareness and the infrastructure for waste water treatment at many places are lagged, which worsened the scenario. On the other hand, the accessible water resource on earth is scarce. It is a well-known fact for many people that only about 2.5% of the water on earth are fresh water, while 1.7% of them are locked in ice caps [3]. The traditional water resource that we depend on comprises only a tiny portion of the total global water and is no longer optimistic to hold up for the development of human being.

People have been looking for "untraditional" water resources to alleviate the confliction between water resource scarcity and water demand. Naturally, seawater drew people's attention with its abundance and availability. Seas and ocean comprise approximately 96.5% of all the water on earth, and would make great water resources if reliable and affordable desalination methods are implemented. The first large-scale desalination technique was thermal desalination [4]. Processes such as multi-effect distillation and multi-stage flash distillation were first utilized and are still being widely used in Middle East [4, 5]. Membrane desalination was not widely recognized until the 1960s [6]. Nevertheless, since then it gradually surpassed thermal desalination and became the most used desalination method world-wide.

Membrane desalination has many advantages over thermal desalination, such as low thermal and electrical energy consumptions and less environmental impacts [4]. However there is one problem that have largely impeded the implementation of membrane desalination technology, and that is membrane fouling. Membrane fouling causes severe permeate flux and quality decline, and increases energy consumption. Many researches and studies have been done focusing on different aspects of fouling issues. And even though our understandings of fouling have

improved, it still remains a major problem for membrane treatments. It is meaningful to look into the field of membrane fouling, to try to understand the underlining factors governing the interactions that cause fouling, and try to find ways to alleviate this issue.

The current research aims at elucidating the interaction between functional groups typically found on polyamide RO membrane surface, and alginate, a major organic foulant for RO desalination, under various solution conditions simulating seawater ionic composition, and relating RO membrane surface chemistry to alginate fouling behavior.

The research consists of two parts. In the first part, self-assembled mono-layers (SAMs) with desired ending functional groups were used to investigate the effect of membrane surface chemical functionalities on alginate adsorption. Alginate adsorption on SAMs and desorption during the subsequent chemical cleaning were measured using Quartz Crystal Microbalance with Dissipation (QCM-D). Initial adsorption rates, equilibrium adsorption mass and cleaning efficiency on different SAMs were compared under well-defined solution conditions. The roles of different electrolyte cations were investigated.

In the second part, lab-scale cross-flow filtration experiments were conducted using commercial RO membranes of different surface properties. The fouling behaviors of the membranes were compared in accordance with their surface properties to determine the role of membrane surface chemical functionalities on alginate fouling.

2, Literature Review

2.1, Membrane fouling

To precisely define membrane fouling is very complicated and difficult, because the characteristics of fouling would differ with different membranes and feed water qualities[2]. However it is generally accepted that membrane fouling is a phenomena which the resistance of the mass transfer across the membrane increases, and the overall performance (e.g. flux, rejection, permeate qualities) dramatically decreases [4]. The causes of fouling also vary, but they can be categorized into the following types: the precipitation of dissolved inorganic salts; the transport of organic matter and colloids; and biological growth [4, 7]. The materials that would cause fouling (namely, foulants) accumulate at the surface of the membrane and form a continuous layer which can impede mass transfer across the membrane. And as it develops to the stage where mass transfer is greatly inhibited, fouling occurs.

2.1.1, Scaling

Scaling generally refers to the precipitated inorganic salts building a thin layer at the surface of the membrane and inhibiting mass transfer across the membrane. In seawater desalination process and other pressure-driven membrane treatments, scaling is mostly caused by concentration polarization

[8]. Concentration polarization describes the phenomena that at the surface of the membrane there is a higher concentration of rejected substances than in the bulk solution. It can be easily understood as at steady state of RO membrane treatment, the diffusion of the rejected substance away from the membrane must be in equilibrium with the convective diffusion toward the membrane. So there exists a negative concentration gradient from the membrane surface to the bulk solution, hence the concentration polarization. Because of this polarization, the rejected salt may become supersaturated and precipitate at the membrane even though the bulk concentration is not saturated [8]. Some of the common substances in seawater that could cause scaling are $CaCO_3$, $CaSO_4$, $BaSO_4$ and silica [4]. Scaling can be inhibited during pretreatment of the feed water by pH adjustment and adding antiscalants [9, 10]. Usually maintaining a pH level of 4-6 of the feed water by adding H_2SO_4 would control the precipitation of carbonates [7]. Antiscalants addition is also very common in membrane desalination processes. The antiscalants hinder scale formation by interfering with the crystallization processes[10].

2.1.2, Bio-fouling

Biological fouling, or bio-fouling, is very common in seawater desalination with feed waters of high microorganism growth potential. Nearly all seawaters would contain microorganisms such as bacteria, fungi, algae, viruses, etc [4]. Bio-fouling generally refers to the biological growth on the surface of the membrane and the consequential negative effects, including formation of biofilm at the surface, production of extracellular polymer substances (EPS) and degradation of membrane material, which in turn would cause severe performance decline in RO desalination [4, 11, 12]. Bio-fouling is especially difficult to eliminate because microorganisms can reproduce. Even if 99% of the microbes in the feed water are killed, the remaining 1% , once attached to a favorable condition at the membrane surface, is still capable of causing bio-fouling. One of the most common method of bio-fouling control is the addition of biocide as pretreatment, such as chlorine. However chlorine injection would cause chemical degradation of the membrane. Research have also been done to optimize and minimize the chlorine dosage for disinfection of feed water[13]. Other sterilization methods can also be seen in RO desalination pretreatment, such as NH_2Cl, ClO_2, O_3, and UV[12]. However the same problem of membrane oxidation degradation exists and the condition and dosage need to be optimized.

2.1.3, Organic fouling

Compared with inorganic matters (with concentration of about 40,000-50,000 ppm), organic matter concentration in the seawater are nearly negligible (of about 2-4 ppm) [14]. However, they can pose serious problems. Researchers have found that positively charged, high molecular mass humic substances are likely to deposit on the membrane surface and form a thin organic layer, causing fouling, especially in hydrophobic membranes [4]. Not only can organic matters foul membrane by themselves, there are also synthetical effects of fouling between organic matters and metal ions such as Calcium ions and Iron ions. Humic acids and alginate can form a gel like fouling layer by complexation of multivalent ions [15]. And irreversible fouling can occur with complexation of calcium, which would form a compactable floc-like structure [15-17]. Also with the presence of divalent ions such as calcium the rate of adsorption of organic matters onto the membrane would increase [16, 18, 19]. So the synthetical effects of organic matters and metal ions not only accelerate the formation of the fouling, they also make the fouling more persistent and even irreversible. Moreover an integral mechanism of fouling may be the complex interactions between dissolved organic matter and colloidal particles [20]. Deposition of colloidal particles would help the adsorption of dissolved organic matters,

moreover colloidal and organic mixture could increase cake layer resistance and hinder foulant back diffusion, which effectively impede water flow [20]. The mechanisms of organic fouling actually vary with different researches results [7]. Some scientists suggested that organic fouling may occur not only on the surface of the membrane, but also inside the membrane, in the "pores" of the membrane, which is more serious and irreversible. Some other scientists disagreed, and interpret the phenomena as reversible sorption within the membrane or irreversible adsorption onto the surface. There are also researches done from the aspect of foulant-membrane physicochemical interactions. Based on force analysis they found out that permeation drag forces is negligible compared with other interfacial forces such as acid-base interaction forces, which is the dominant force [21].

2.2, Membrane surface properties and fouling

2.2.1, Surface physical chemical properties and fouling

There are many factors that influence membrane fouling, for example feed water conditions such as the presence of calcium ions that could affect organic fouling as mentioned in the previous section. Other factors are also important including membrane surface characteristics and foulant properties

[22, 23]. However in real operations not all factors can be easily controlled. Generally these three factors can be categorized into two groups, selective factors and non-selective factors [22]. Foulant properties and feed water conditions are generally non-selective since they are dependent on the source of water to be treated, and it would usually be economically inefficient to alter those properties. Membrane surface properties, however, is partially selective and could be potentially controlled by the manufacture. So it is important to learn about which membrane surface properties governs the interactions between foulant and membrane so that we could make changes accordingly to alleviate or eliminate fouling in order to achieve better membrane performance.

A lot of studies have been done trying to find out what surface properties would influence membrane fouling. And researchers and scholars have gradually come to realized that there are several surface properties that are important, including membrane surface hydrophobicity, membrane surface charge, and membrane surface roughness [24, 25]. Hydrophobicity of the membrane surface has an important affect in foulant-membrane interactions. Studies have shown that organic foulants, mostly exerting hydrophobic characteristics, would preferentially adhere to membrane surfaces that are also hydrophobic [26]. Surface charge also influences

membrane-foulant interaction through electrostatic interactions. Since most of the natural occurring organic or colloidal foulants generally possess negative charges at the surface, membrane surfaces that exhibit more electric negativity would have less fouling tendency due to the electric double layer repulsion between membrane and foulants [24]. Last but not least, surface roughness of the membrane could be prominent in organic or colloidal fouling. Many studies were able to correlate membrane fouling by organic or colloids with surface roughness of the membrane [27, 28]. In some cases, it was shown that roughness had more dominant influence over other surface properties [29]. There are many reasons that roughness would contribute to fouling. First of all the "valley" structure on the membrane surface would preferentially accumulate foulants. Then once the foulants get in to the "valley", they are less influenced by the hydraulic shear forces and are harder to be removed. Also, a rougher surface provides more surface area for foulant to adhere to, which then increases fouling [29].

2.2.2, Membrane chemical composition and fouling

Besides the membrane characterizations stated above, there is another important aspect that not only affects fouling, but also interlinks all the above characterizations. And that is membrane surface active layer chemical

composition. For most commercial reverse osmosis membranes, the top active layer is formed by interfacial polymerization of aromatic amine monomers and aromatic carboxylic acid chloride monomers [30]. And one of the most commonly used recipe for creating a selective layer is by interfacial polymerization of 1,3-benzenediamine and trimesoyl chloride to form a fully aromatic polyamide layer [31] (Figure 1). Other monomers such as 1,4-benzenediamine, 1,3,5-benzenetriamine, 1-isocyanato-3,5-benzenedicarbonyl etc., are also used [2]. The formed polyamide will have distinct surface morphology characteristics and show certain degree of roughness, known as the ridge-and-valley structure [31]. Also from the reaction scheme we can see that different types of functional groups are involved in the reaction, which suggests that the charge property of the formed polyamide will be strongly influenced by the presence and state of the functional groups [32]. Study has shown that there are inter-relationships between surface properties and for uncoated membrane they are largely determined by the polyamide chemistry [32, 33].

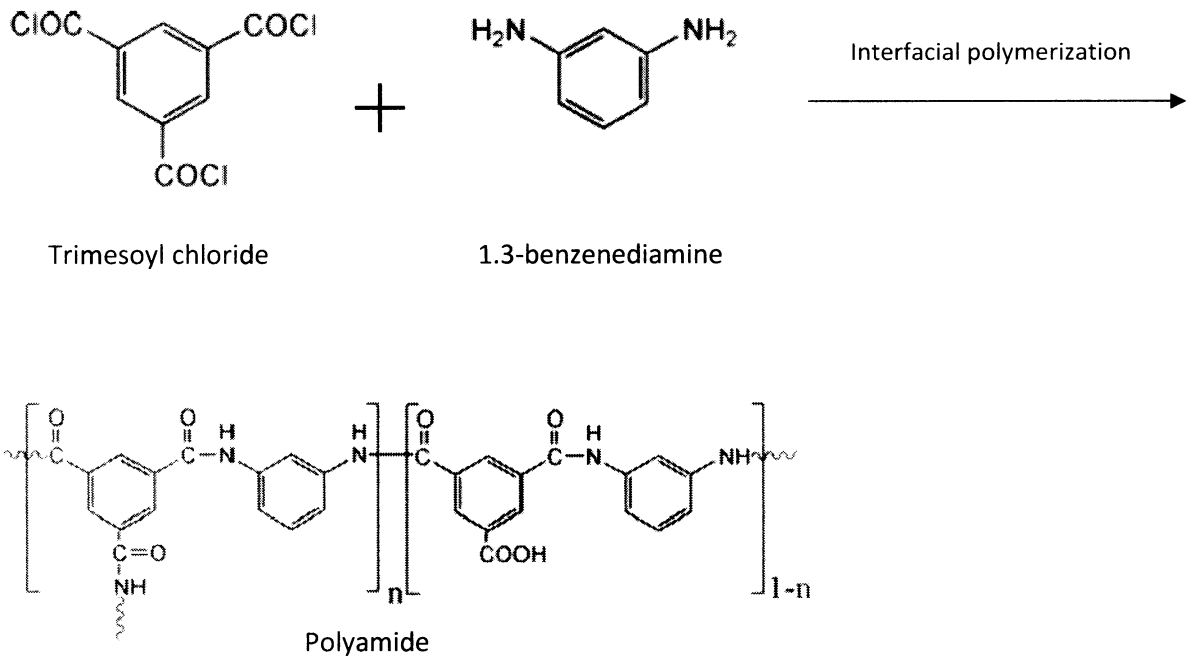

Figure 1 Typical formation of thin film composite fully aromatic polyamide active layer

As a matter of fact, membrane chemistry and chemical composition not only influence the physicochemical properties of the surface, but also affect membrane fouling directly, through the specific interactions between functional groups on the membrane and in the foulants. Limited studies have been done studying the specific interaction of polyamide membrane functional groups though [34], due to the chemical heterogeneity on the membrane surface. But specific interactions between functional groups typically found on the membrane surface and in typical organic foulants, such as $-NH_2$ and –COOH, are evident and have been found in many other researches [35, 36]. So it is eminent that methods to be found that could isolate different membrane functionalities and monitor the interaction

between foulants and the functionalities, and shed light on the influence of membrane surface functionality on fouling.

2.3, Quartz Crystal Microbalance with Dissipation (QCM-D) Technology

The merits of QCM-D technology are that it enables the study of interactions on surfaces with specific chemistry, and it is capable of monitoring the minute changes in adsorbed mass. The basic theory of QCM-D is based on the principle that when a quartz crystal in gaseous or liquid environment is excited, it oscillates at a fundamental frequency (~5 MHz). As absorbates attach onto the crystal surface, the resonant frequency of the crystal decreased with the increased amount of attachment. The Sauerbrey model (Eq. 1) describes the relationship between the shift in frequency and the absorbed mass per unit surface area of the crystal under four assumptions: 1), the absorbed mass is evenly distributed; 2), the adsorbed layer is rigid enough to have no energy dissipation; 3), the adsorbed layer is thin enough that the internal friction is negligible; 4), the absorbed mass is small compared with that of the quartz crystal [37].

$$\Delta m = -\frac{C \cdot \Delta f}{n} \quad (1)$$

Where Δm is the change of adsorbed mass on the surface

Δf is the change of the frequency of the quartz crystal

C is the mass sensitivity constant (=17.7 ng/(cm^2·Hz) at f = 5 MHz)

n is the overtone number

However, the Sauerbrey model is not valid when the assumptions are not met. For the adsorption of most proteins or polysaccharides, the layers are highly viscoelastic and can cause significant energy dissipation. Thus, energy dissipation as well as frequency change should be considered in order to accurately interpret the mass change and the structural change of the adsorbed layer [37].

Dissipation factor is defined as [37]:

$$D = \frac{E_{dissipated}}{2\pi E_{stored}} \quad (2)$$

Where D is the sum of the energy dissipated in the oscillation system

$E_{dissipated}$ is the dissipated energy

E_{stored} is the energy stored in the oscillation system

When the driving power to a piezoelectric crystal oscillator is switched off, the crystal oscillation decays as an exponential damped sinusoidal (Eq. 3)[38].

$$\mathrm{A(t)} = A_0 e^{\frac{t}{\tau}} \sin(2\pi f t + \varphi) \tag{3}$$

Where A is the amplitude

τ is the decay time constant

f is the frequency

φ is the phase angle

The decay time constant is related to the dissipation [38]:

$$D = \frac{1}{\pi f \tau} \tag{4}$$

Where f is the frequency

τ is the decay time constant

The QCM-D instrument monitors the shift of frequency (Δf) and dissipation (ΔD) of the quartz crystal by recording the voltage amplitude during the decay and numerically fitting the curve to the above relationships. The Δf and ΔD information are then used, in combination with viscoelastic

models, to interpret the mass and the viscoelastic properties of the adsorbed layer. In QCM-D, the most commonly used model for assessing the adsorbed viscoelastic layer is the Kelvin-Voigt model[37], which is represented by a purely elastic spring connected with a purely viscous damper in parallel. The model can be expressed as [39]:

$$\frac{d\varepsilon}{dt} = \frac{\sigma}{\eta} - E\frac{\varepsilon}{\eta} \tag{5}$$

Where σ is stress in the system

ε is strain within the system

E is a modulus of elasticity

η is viscosity

A typical scheme for the QCM-D system, as depicted in Figure 2, assumes a thin polymer layer on top of the rigid crystal surface. The homogeneous layer covers the entire area of the crystal surface and the thickness is uniform. The properties of the layer such as density, viscosity, elasticity and thickness can then be correlated with Δf and ΔD with Kelvin-Voigt model. Researchers have solved the general solution for the wave equation of shear waves in viscoelastic layer on the quartz crystal surface.

The acoustic response of the quartz crystal with adsorbed viscoelastic layer in a Newtonian bulk liquid can be described as [40]:

$$\Delta f \approx -\frac{1}{2\pi\rho_0 h_0}\left\{\frac{\eta_3}{\delta_3} + h_1\rho_1\omega - 2h_1\left(\frac{\eta_3}{\delta_3}\right)^2 \frac{\eta_1\omega^2}{\mu_1^2+\omega^2\eta_1^2}\right\} \quad (6)$$

$$\Delta D \approx \frac{1}{2\pi f\rho_0 h_0}\left\{\frac{\eta_3}{\delta_3} + 2h_1\left(\frac{\eta_3}{\delta_3}\right)^2 \frac{\mu_1\omega}{\mu_1^2+\omega^2\eta_1^2}\right\} \quad (7)$$

Where ρ_0, h_0 are the density and thickness of the crystal respectively

η_3 is the viscosity of the bulk liquid

δ_3 is the viscous penetration depth of the shear wave in bulk liquid

ω is the angular frequency of the oscillation

ρ_1, μ_1, η_1, and h_1 are the density, shear elasticity, viscosity and thichness of the adsorbed layer, respectively

During the modeling of QCM-D experiments, the viscoelastic property values of the adsorbed layer were numerically fitted within pre-defined ranges by combining the monitored Δf and ΔD at multiple overtones with equation 6 and 7 via computer calculation.

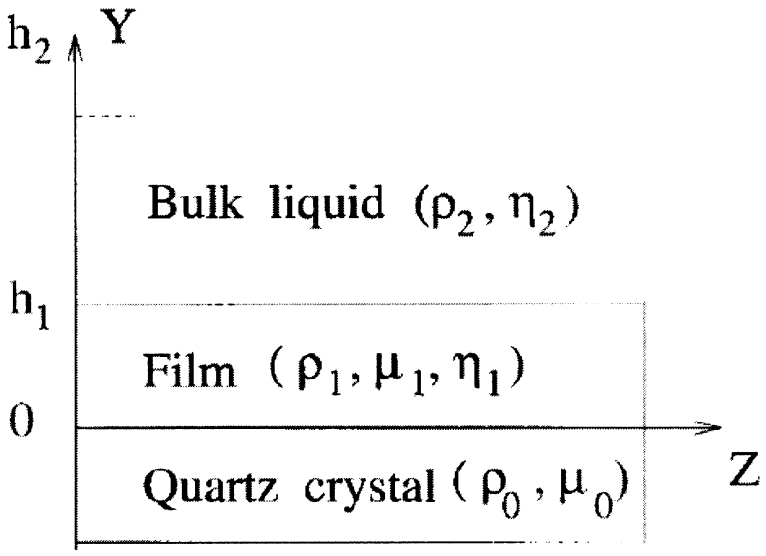

Figure 2 Geometry of a quartz crystal microbalance covered by a single-layer viscoelastic film oscillating in a bulk liquid (figure adapted from [40])

3, Materials and Methods

3.1, QCM-D experiments

3.1.1, Materials

(1), Salt solutions and alginate solutions

Salt solutions in the QCM-D experiments were made from reagent grade NaCl, $MgCl_2 \cdot 6H_2O$, $CaCl_2 \cdot 2H_2O$ and HCl (purchased from Sigma Aldrich, St. Louis, MO), as well as a commercial sea salt Instant Ocean (Spectrum Brand, Inc., Madison, WI). Ultrapure water (R≥18.1 megaΩ-cm) generated by an E-Pure system (Barnstead, Batavia, IL) was used in making all solutions. Four solutions were made for QCM-D experiments, namely Na^+, $Na^+ + Mg^{2+}$, $Na^+ + Ca^{2+}$ and Seawater. Seawater solution was made by dissolving 32 g Instant Ocean sea salt in 1 L of ultrapure water, stirring for 6 hr, and then filtering through a 0.45 μm membrane. The concentration of major cations (Na^+, Mg^{2+}, and Ca^{2+}) were measured using ICP-OES. In order to study the interaction between alginate and membrane functional groups under desalination conditions and the roles of different cations, we designed three different electrolyte solutions: 1) the Na^+ (in the form of NaCl) solution, without any divalent cations, and of the same ionic strength as the Instant Ocean solution; 2) the $Na^+ + Mg^{2+}$ solution, with Mg^{2+} (in the form of

$MgCl_2$) at the same concentration as that in the Instant Ocean solution, and NaCl making up the ionic strength; 3) the $Na^+ + Ca^{2+}$ solution, with Ca^{2+} (in the form of $CaCl_2$) at the same concentration as that in Instant Ocean solution and NaCl making up the ionic strength. The ionic strength of 32 g/L Instant Ocean solution was obtained from [41]. The pH for all solutions was adjusted using 0.2 M HCl to 6.0 ± 0.5. The Na^+, Mg^{2+} and Ca^{2+} concentrations as well as total ionic strength for each solution were summarized in Table 1.

Table 1 Na+, Mg2+ and Ca2+ concentrations and total ionic strength of solutions

	Na^+ (M)	**Mg^{2+} (M)**	**Ca^{2+} （M）**	**Ionic Strength (M)**
Na^+	0.6284	—	—	0.63
$Na^+ + Mg^{2+}$	0.4851	0.0478	—	0.63
$Na^+ + Ca^{2+}$	0.6014	—	0.0089	0.63
Seawater	0.4558	0.0484	0.0090	0.63 [41]

Alginate solutions for the QCM-D experiments were made by dissolving alginate stock solution in the salt solutions Na^+, $Na^+ + Mg^{2+}$, $Na^+ + Ca^{2+}$ and Seawater, to achieve a concentration of 100 mg/L. Sodium alginate derived from brown algae was purchased from Sigma-Aldrich (St. Louis, MO). The 2 g/L alginate stock solution was made by dissolving 400 mg alginate in 200 ml ultrapure water then vigorously stirring overnight, and

the solution was stored at 4°C. All alginate solutions were made at least 24 hr prior to QCM-D experiment and stored at 4°C. Solutions were brought to room temperature before each experiment.

(2), Alkanethiol solutions

Alkanethiol solutions were used to produce SAM layers on gold surface with desired end groups. Four alkanethiols, namely 1-Dodecanethiol, 11-Mercaptoundecanoic acid, 11-Mercaptoundecanamide and 11-Amino-1-undecanethiol hydrochloride (Figure 3), were purchased from Asemblon (Remond, WA). Thiol solutions were made by dissolving certain mass/volume of the alkanethiol in 200 proof ethanol to achieve the concentration of 1 mM. For liquid thiol, in our case 1-Dodecanethiol, a density of 0.84 g/ml was used in calculating the volume of liquid thiol need.

(3), Cleaning solution

Cleaning solution used in QCM-D experiments was 2% Sodium Dodecyl Sulfate (SDS) solution with unadjusted pH of ~9. It was made by dissolving 20 g of Sodium Dedecyl Sulfate (IBI Scientific, Peosta, IA) in 980 ml ultrapure water. The solution was stirred and briefly heated to help dissolution.

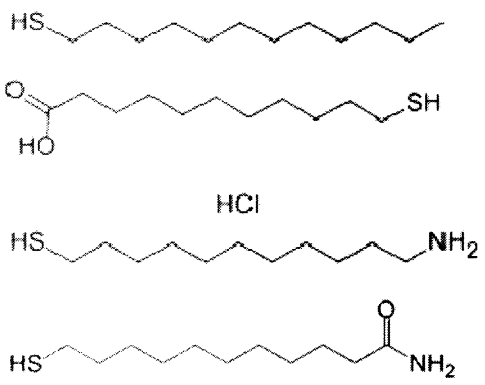

Figure 3 Molecular structures of the alkanethiols in the experiment

3.1.2, Methods

(1), Preparation and characterization of SAM layers

SAM-layers were prepared on gold-coated QCM-D crystals. Prior to SAM-layer preparation, QCM-D crystals were cleaned by sonicating twice each in toluene, acetone and ethanol, respectively, in a sonication bath (Bendeline Sonorex, London, England), 10 min each time. After that the crystals were dried with ultra-pure nitrogen and put in an UV/ozone chamber (ProCleaner Chamber, Bioforce Nanoscience, Ames, IA) for 30 min. Contact angles of pure water on cleaned surfaces were measured to ensure the effectiveness of cleaning. For SAM-layer assembly, cleaned crystals were first put in 1 mM alkanethiol solutions of desired end groups and immersed for 24 hr. For 11-Mercaptoundecanoic acid and 11-Amino-1-

undecanethiol solutions, pH was adjusted to 2 and 11 respectively using 0.2 M HCl and 30% NH_4OH to reduce the electrostatic repulsion between the alkanethiol chains, thus facilitate the formation of a more orderly SAM-layer. After the first immersion step, the crystals were transferred and immersed in 1 mM dodecanethiol solutions for another 24 hr to achieve a better coverage and more homogeneous layer. Before each of the immersion steps, the solutions were purged with pure argon to remove dissolved oxygen that could oxidize the alkanethiols. After the immersion steps, the crystals were thoroughly rinsed with 200 proof ethanol and dried with ultrapure nitrogen.

Static water contact angle in air were measured on each SAM-layer using the sessile drop method with CAM 200 contact angle analyzer (KSV instrument LTD, Helsinki, Finland). Contact angle values used were averages of left and right contact angles and five measurements were made on each crystal.

(2), Characterization of alginate in salt solutions

Zeta potential and particle size of alginate in different salt solutions were measured at an alginate concentration of 100 mg/L. Zeta potential was determined by electrophoretic mobility measurement and particle size was characterized as hydrodynamic diameter by dynamic light scattering. Six

and four measurements were made for particle size and zeta potential, respectively. Measurements were carried out using a Zetasizer Nano ZS (Malvern Instruments, Westborough, MA).

(3), Adsorption experiments

Adsorption experiments were carried out using QCM-D (Q-Sense E4, Q-Sense, Glen Burnie, MD). A freshly prepared SAM coated QCM-D crystal was mounted in each flow chamber, and the test solution was pumped through the flow chamber at desired flow rates. The QCM-D instrument monitored the changes in the resonant frequency (Δf) and dissipation (ΔD) of the quartz crystals at different resonance overtones, and the shifts were used to model the adsorbed layer properties. Experiments were conducted in a controlled temperature of 25 °C. The flow rate was controlled by a high precision multichannel pump dispenser (Labinett lab AB, Goteborg)

For each QCM-D experiment, Δf and ΔD baselines were first established in air, pure water, and then salt solutions before alginate solutions were introduced into the flow chambers. The flow rate of pure water and salt solutions was controlled at 50 μl/min, which exerted a flow velocity of approximately 0.1 mm/s on the crystal surface (estimated by

assuming a rectangular flow channel with length of the diameter of the crystal), and a Reynold number of around 0.1 with pure water. Baselines allowed us to determine if the system was stable and to avoid any significant drifts in frequency and dissipation. After stable baselines were established in the salt solution, the feed was switched to an alginate solution to carry out the adsorption experiment. The flow rate of the alginate solution was kept the same at 50 μl/min. Obvious shifts in Δf and ΔD could be observed when the feed was switched to the alginate solution. After a certain period of time when Δf and ΔD were stable and constant, adsorption equilibrium was assumed. The feed was then switched back to the background electrolyte solution to eliminate the bulk viscosity effect (the shift in frequency and dissipation caused by the difference in viscosity between the alginate solution from and the background electrolyte solution).

The next step of the experiment was to switch the solution to 2% SDS to conduct cleaning. Cleaning was carried out in the same flow rate of 50 μl/min. The SDS solution was pumped to the flow chambers until Δf and ΔD were stable and constant. Then it was switched to the background electrolyte solutions at the same flow rate to remove bulk viscosity effect. After that pure water was pumped into the system at 0.1 ml/min to clean the system.

(4), QCM-D modeling

The purpose of QCM-D modeling was to translate the shifts in frequency and dissipation of the quartz crystal into information on the absorbed layer properties. For a single-layer viscoelastic film in the QCM-D system, as depicted in Figure 2, six parameters were used to describe the geometry: density (ρ_1), viscosity (η_1), shear elasticity (μ_1), and thickness of the adsorbed layer, and viscosity (η_2) and density (ρ_2) of the bulk fluid . The parameters were related to the shift in frequency and dissipation through wave equations describing the propagation and decay of shear waves in visco-elastic materials. The Kelvin-Voigt model was used to describe the visco-elastic property of the adsorbed layer. A detailed description of the QCM-D theory can be found in [40].

QCM-D modeling was done using a software (Q-tool) provided by Q-sense. A single layer Voigt visco-elastic model was used to model all of the layers in the experiments. For most experiments, frequency and dissipation shifts at overtones from the third to the eleventh were used in the modeling. In a few experiments, data obtained at some overtones exhibited deviated behaviors compared with the rest and were disregarded from modeling. Six parameters were included in the model to represent the conditions in the

QCM-D cell. Three of them were fixed parameters including fluid density, fluid viscosity and adsorbed layer density, and the other three are fitted parameters including adsorbed layer viscosity, adsorbed layer shear elasticity and adsorbed layer thickness (or mass). Fluids in the model refer to the background bulk solution for the adsorption experiment, as described in 3.1.1. Densities of the solutions were all estimated base on their recipes (assuming the addition of salts does not change the total volume of the solution). Viscosities of the solutions were obtained by QCM-D methods described in their support manuals [42], and were set at 0.00095 kg/(m·s) for all solutions (at 25 °C). The viscosity of salt solutions showed a slight increase compared with that of pure water (~0.00089 kg/m·s). Density of the absorbed layer was estimated to be 1050 kg/m^3, based on the model fitting results. The ranges for fitted parameters were set at 0.01 to 0.0015 kg/ms, 1000 to 1E8 Pa, and 10 to 1E5 ng/cm^2 for adsorbed layer viscosity, shear elasticity and mass, respectively.

3.2, Filtration experiments

3.2.1, Materials

(1), Seawater solution, alginate solution and cleaning solution

Feed water in the lab-scale cross-flow filtration experiments were Instant Ocean seawater solutions. The seawater solutions used in this experiment were the same as the seawater solutions used in the QCM-D experiments, made by dissolving 256 g of Instant Ocean into 8 L of ultrapure water, filtering through 0.45μm filter and adjusting pH.

Alginate solutions were made by adding alginate stock solutions into the seawater solution to achieve a concentration of 100 mg/L. Alginate stock solution of a concentration of 20 g/L was made by dissolving 4 g sodium alginate into 200 ml of ultrapure water and vigorously stirred overnight.

The cleaning solution used in the filtration experiment was 2% SDS solution, made by dissolving 120 g SDS into 6 L of ultrapure water and stirred overnight.

(2), Commercial reverse osmosis membranes

Four commercial membranes were used in the filtration experiments, SWC5 membrane from Hydronautics (Oceanside, CA), SHF and SN

membrane from CSM filter (Woongjin Chemical, Irvine CA), and TM820C membrane from Toray (Poway, CA). According to the manufactures, these membranes are all fully aromatic thin film composite polyamide membranes. Their specifications are summarized in Table 2.

Table 2 Specification information of the membranes from the manufacture

	Hydranautics	**CSM filter**		**Toray**
	SWC5	SHF	SN	TM820C
Test Conditions				
Feed water Pressure (psi)	800	800	800	800
Feed water Temperature (°C)	25	25	25	25
Feed water Concentration (mg/L NaCl)	32000	32000	32000	32000
Recovery Rate (%)	10	8	4	8
Feed water pH	6.5-7.0	6.5-7.0	6.5-7.0	8
Area (m^2)	37	2.2	3.3	34
Test Results				
Permeate (m^3/day)	34	2.3	2.3	22.7
Salt Rejection (%)	99.8	99.7	99.2	99.75
Permeability (m/s·psi)	1.33×10^{-8}	1.51×10^{-8}	1.00×10^{-8}	9.66×10^{-9}

The membrane samples were received as flat sheets and were prepared by cutting the membranes into approximately 1.5 inch by 3 inch coupons, thoroughly rinsing with ultrapure water and storing in ultrapure water at 4°C. All membranes were soaked for at least 24 hr prior to their experiments, and water was changed regularly.

3.2.2, Methods

(1), Membrane surface characterization

Both the surface physical and chemical properties of the membranes were characterized, including hydrophobicity, surface roughness, and chemical compositions. Hydrophobicity of the membranes was characterized by sessile drop water contact angle measurement described in section 3.1.2. Both deionized water and seawater solution were used as the liquid probe. Contact angles were averages of left and right contact angles and ten measurements were made on each sample. Membranes were soaked in deionized water for at least 24 hr, dried in vacuum for at least 72 hr prior to experiments.

Surface roughness of the membranes was characterized by a multimode atomic force microscopy (AFM) (Veeco, Santa Barbara, CA). Characterizations were carried out both in air and in seawater. Surface roughness in air was measured by tapping mode AFM. Membranes were not rinsed or soaked prior to roughness measurement in order to prevent deformation by swelling and drying, but were cleaning by blowing with pre-purified nitrogen gas. Surface roughness in seawater was measured by contact mode AFM with silicon nitride probes (NP-S10, Veeco, Santa

Barbara, CA). Membranes were not soaked in deionized water prior to experiments, but were equilibrated with seawater in the fluid chamber for approximately 20 min before each measurement. Surface roughness was represented by the root mean square (RMS) roughness over $10\times10\mu m^2$ areas on the membranes and was averaged over three measurements for each condition.

Chemical compositions of the membranes were characterized by both attenuated total reflection-Fourier transform infrared spectroscopy (ATR-FTIR) and X-ray photoelectron spectroscopy (XPS). FTIR measurements were carried out using a Nicolet Nexus 470 FTIR spectrometer equipped with an Attenuated Total Reflection element and an Omnic software. Twelve replicate spectrums were obtained for each membrane sample on random sites. Each spectrum was averaged over 64 scans and covered wave number from 650 to 4000 cm^{-1} at 2 cm^{-1} resolution. Background subtraction and baseline adjustment were carried out on each measurement. Elemental compositions of the membranes were analyzed by XPS (Thermo Fisher Scientific Inc., Waltham, UK) with an Al x-ray source and a monochromator.

(2), Lab-scale cross-flow filtration experiments

Filtration experiments were conducted in a lab-scale cross-flow membrane filtration system depicted in Figure 4. Feed water was continuously mixed in the feed tank during the filtration experiment by a suspended magnetic stirrer. The temperature of the feed water was controlled at 20°C by circulated water in a stainless steel coil submerged in the feed water cooled by a re-circulating water chiller (VWR Inc., West Chester, PA). A hydra-cell pump (D-03, Wanner Engineering Inc., Minneapolis, MN) supplied the feed water to two identical parallel plate and frame membrane cells with channel dimensions of 6.25 cm × 2.45 cm × 0.51 cm. A pulsation dampener (H1020V, Blacoh Fluid control Inc., Riverside, CA) was installed at the outlet of the pump to regulate pressure pulses. The cross-flow of the feed was controlled at a constant flow rate of 1 L/min by a bypass valve, and the trans-membrane pressure was controlled by a back-pressure regulator. Permeate flux from the two membrane cells was monitored by a digital flow meter (Optiflow 1000, Agilent Technology Inc., Foster City, CA) and was automatically recorded to a lab computer. Both the permeate and the retentate were recycled to the feed tank to maintain the feed water concentration.

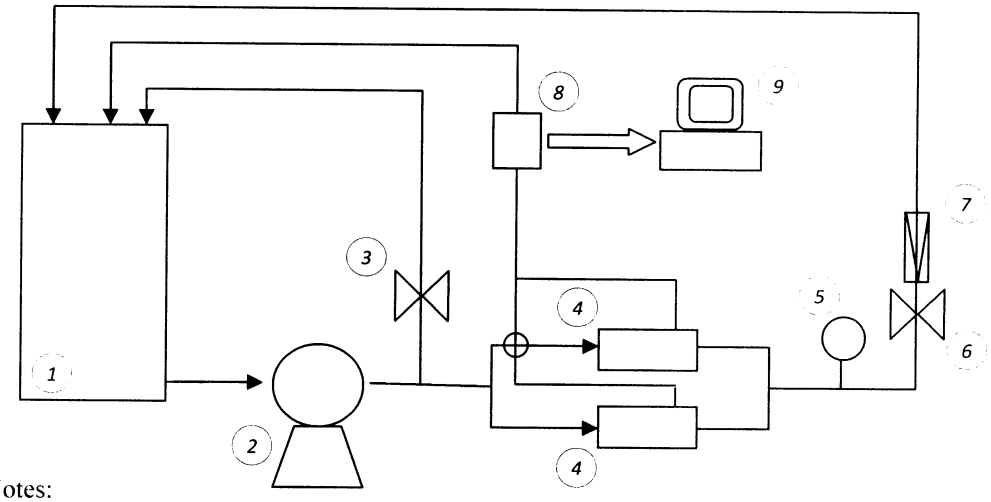

Notes:

① Feed tank

② Feed pump

③ Bypass valve

④ Membrane cells

⑤ Pressure gauge

⑥ Back-pressure valve

⑦ Flow meter (cross-flow rate)

⑧ Digital flow meter (permeate flow rate)

⑨ Computer

Figure 4 Schematic of the lab-scale cross-flow filtration system

The filtration experiment protocol consists of four steps, including membrane compaction with ultrapure water, membrane conditioning with artificial seawater solution, membrane fouling with alginate solution, and membrane cleaning with 2% SDS. At the beginning of each experiment, membranes were compacted by running the filtration experiment with ultrapure water in a pressure higher than the designed pressure for at least 5 hr until a stable flux was obtained. After compaction, pump was stopped and feed water was replaced with the artificial seawater solution. Conditioning was carried out by filtering seawater solution for at least 9 hr. The applied

pressure was adjusted to obtain a stable permeate flux of 5.5×10^{-6} m/s for all experiments. Feed pressures ranging from 421 psi to 570 psi were applied to different membranes to achieve the desired permeate flux. Both feed and permeate were sampled at different times for conductivity measurement, and salt rejection was calculated from conductivity of the feed and permeate. After conditioning, the pump was stopped and 40 mL of the 20 g/L alginate stock solution was added to the seawater solution to achieve the designed foulant concentration of 100 mg/L. The feed solution was stirred for 30 min to ensure good mixing before filtration started. Samples were taken at designed time points during the fouling experiment for analysis of pH, conductivity (Oakton pH/CON 510 Benchtop Meter, Oakton Instruments, Vernon Hills, IL) and TOC (Shimadzu Scientific Instruments, Japan).

Fouling experiment was considered complete when flux became stable and showed no significant decline. Then the pump was stopped and the feed water was changed to the cleaning solution. Cleaning was done by running the cleaning solution at a cross-flow rate of 1 L/min with no cross-membrane pressure for 2 hr. Then the system was thoroughly rinsed by pumping ultrapure water through the system for six times, 30 min each time, to get rid of the excess cleaning solution. Then ultrapure water was

introduced again with the same applied pressure as that in the compaction phase to measure clean water flux.

4, Results and Discussions

4.1, QCM-D Results

4.1.1, Characterization of SAMs

SAMs were characterized by static water contact angle analysis. XPS and ellipsometry analyses of the SAMs formed following the same protocol are reported elsewhere [43]. XPS measurements confirm the presence of the desired functional groups. XPS and contact angle analyses of the SAMs coated with and without the second step of immersion in dodecanethiol showed that the second immersion step improved the homogeneity of the SAMs although the amount of dodecanethiol absorbed onto the SAMs in this step was very small [43]. Ellipsometry measurements showed that the thicknesses of the SAMs were between 1.2 – 1.5 nm [43].

From the properties of the SAMs summarized in Table 3, we can see that the three SAMs studied, namely –COOH, $–NH_2$, and $–CONH_2$, have very different hydrophobicity, with –COOH and $–CONH_2$ being very hydrophilic and $–NH_2$ being relatively hydrophobic. The standard deviations of water contact angle for all three SAMs were generally close to 10%, which indicates a good formation of homogeneous SAMs.

Table 3 Characteristics of coated SAM-layers

Functional Group	Alkanethiol used	Contact Angle (°)	Thickness [43] (nm)
-COOH	11-Mercaptoundecanoic acid	34.9 ± 4.1	1.25
-NH_2	11-Amino-1-undecanethiol, hydrochloride	62.5 ± 7.3	1.43
-$CONH_2$	11-Mercaptoundecaneamide	41.8 ± 4.3	1.25

4.1.2, Adsorption/deposition of alginate onto SAMs

The adsorption processes were carried out under the protocol and the conditions described in the previous section. We modeled the processes with information of the changes of frequency and dissipation of the QCM-D sensor crystals and interpreted the amount of mass absorbed/deposited onto the surfaces of the SAMs over time, from the initial buffer baseline to the buffer rinsing stage. Figure 5 illustrates one of the modeled results of adsorption/deposition process as an example.

In our study we compared the amount of mass absorbed/deposited onto different SAMs at adsorption equilibrium, as well as the initial adsorption/deposition rate of alginate on different SAMs, under different solution conditions, in order to interpret the factors influencing desalination RO membrane fouling and the potential role of specific functionalities. The mass on the surfaces at equilibrium were taken from the buffer rinsing part

of the curve where the influence of the viscosity difference between the buffer and the fouling solution was eliminated, and the initial adsorption rates were estimated from the initial linear part of the adsorption kinetics curves. All results reported are averages from three experiments.

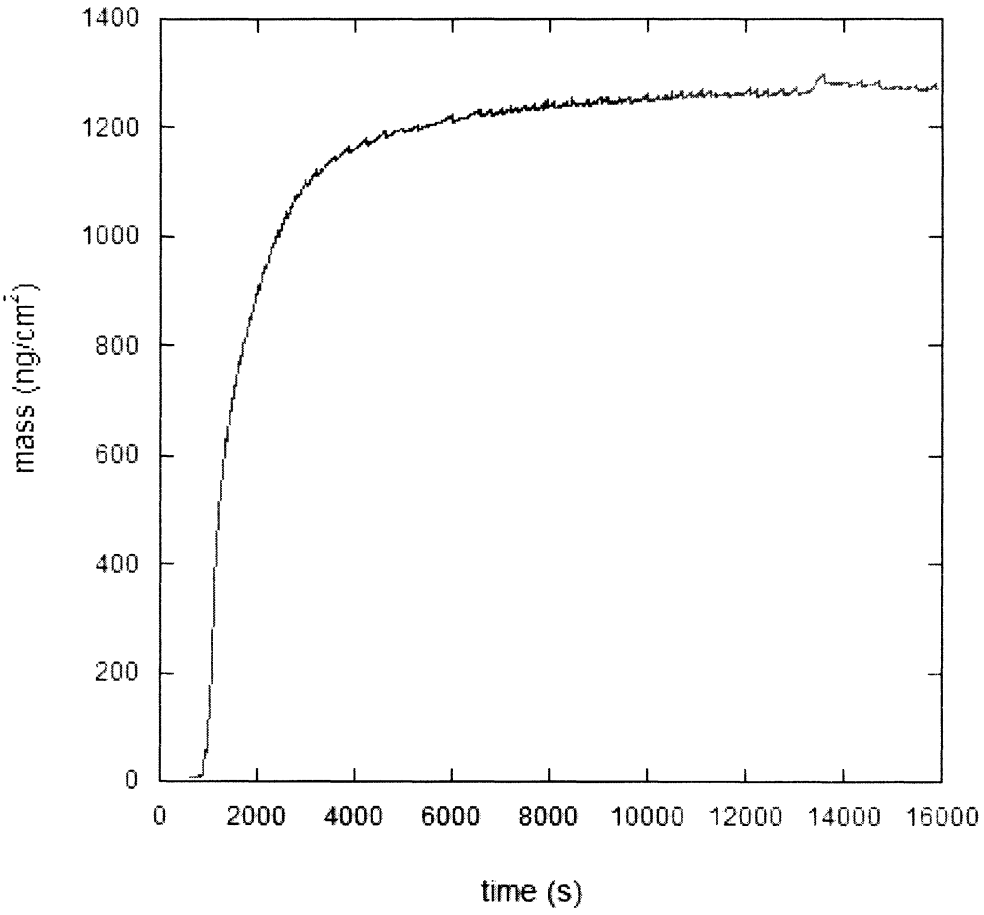

Figure 5 Example of modeled adsorption process (modeled time from ~500s to ~16000s)

(1), Adsorbed/deposited mass at equilibrium

Comparing the absorbed/deposited mass on different surfaces gives us an idea about which functional groups and conditions would have the most fouling. The amounts of mass on the surfaces under different solution conditions are summarized in Figure 6.

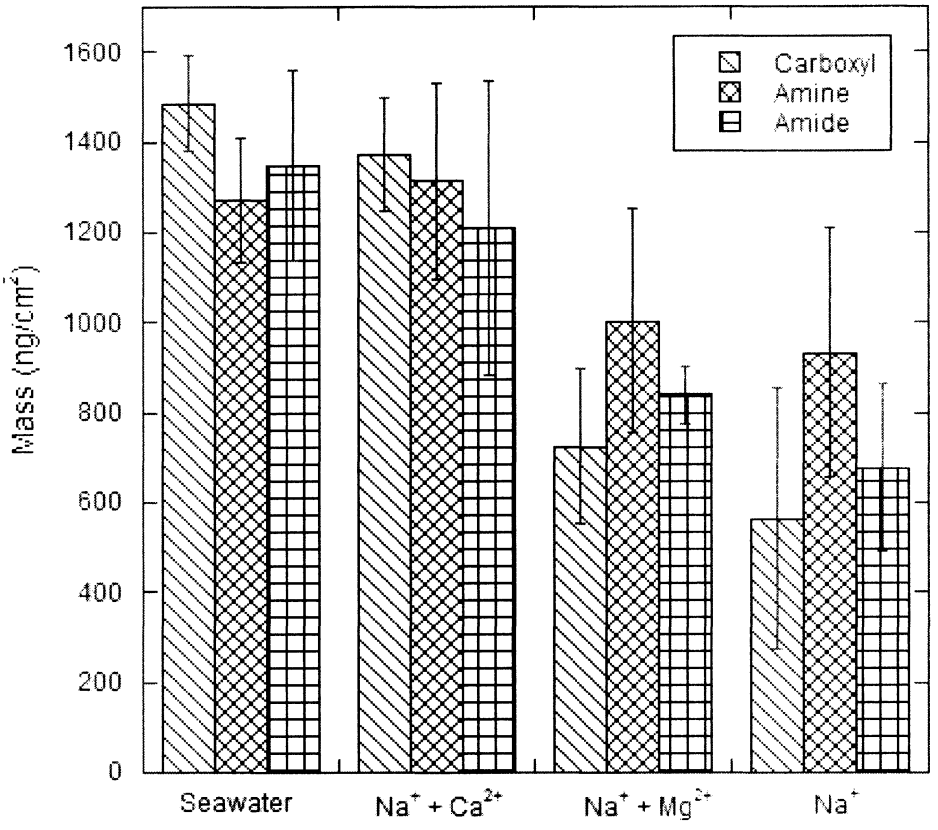

Figure 6 Summary of mass adsorbed/deposited at equilibrium on different surfaces

Table 4 P values (two tailed) of student's t tests comparing (a) the adsorbed/deposited mass in different solution conditions (b) the adsorbed/deposited mass on different SAM surfaces

(a)	Seawater	Na^++Ca^{2+}	Na^++Mg^{2+}	Na^+
-COOH				
Seawater	–	0.29	0.0029	0.0066
Na^++Ca^{2+}		–	0.0063	0.011
Na^++Mg^{2+}			–	0.45
-NH_2				
Seawater	–	0.8	0.18	0.13
Na^++Ca^{2+}		–	0.18	0.13
Na^++Mg^{2+}			–	0.76
-$CONH_2$				
Seawater	–	0.57	0.016	0.015
Na^++Ca^{2+}		–	0.13	0.07
Na^++Mg^{2+}			–	0.23

(b)	–COOH	–NH_2	–$CONH_2$
Seawater			
–COOH	–	0.098	0.37
–NH_2		–	0.63
–$CONH_2$			–
Na^++Ca^{2+}			
–COOH	–	0.71	0.47
–NH_2		–	0.67
–$CONH_2$			–
Na^++Mg^{2+}			
–COOH	–	0.57	0.19
–NH_2		–	0.33
–$CONH_2$			–
Na^+			
–COOH	–	0.19	0.60
–NH_2		–	0.26
–$CONH_2$			–

proved in the particle size measurements of alginate aggregates in different solution conditions (Figure 7). As we can see from the measurement results, particle sizes of alginate aggregates in the artificial seawater and in the Na^+ + Ca^{2+} solution were very similar, suggesting that Ca^{2+}-induced gel-formation is dominant in controlling the particle size of alginate in seawater (Table 5). On the other hand, alginate aggregate sizes in the Na^+ and Na^+ + Mg^{2+} solutions were significantly smaller. Higher degree of aggregation is an indication of enhanced alginate-alginate attraction. This pattern of the distribution of particle sizes coincides with the amounts of absorbed/deposited mass under different solution conditions, suggesting that solution conditions influences the adsorption/deposition of alginate, while Ca^{2+} plays a very important role.

Looking at the over-all data for adsorption in high ionic strength conditions, the total alginate mass absorbed/deposited were significantly (over 50%) higher than those in low ionic strength conditions [43]. Meanwhile, the difference of adsorbed/deposited mass on different SAM surfaces under seawater condition did not show significant difference. This indicates that solution condition is a major factor governing the fouling of alginate on RO membrane surface, while Ca^{2+} dominants the influence by enhancing foulant-foulant attraction. Surface functionality, however, does

not play an important role for the mass of equilibrium adsorption of alginate under seawater condition. It is possibly because that foulant-foulant interaction dominants the fouling process over foulant-surface interaction.

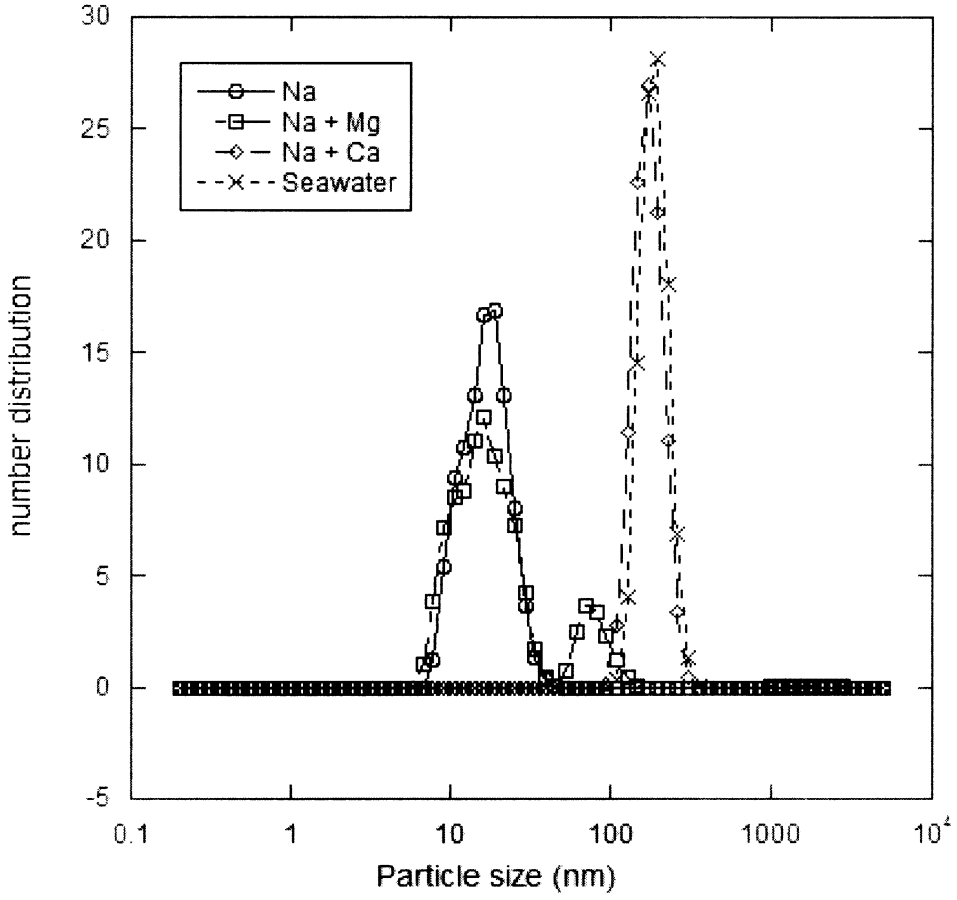

Figure 7 Particle size distribution of alginate under different solution conditions

Table 5 Zeta potentials and average particle sizes of alginate under different solution conditions

	Seawater	Na^++Ca^{2+}	Na^++Mg^{2+}	Na^+
Particle size (nm)	192.28	174.95	27.78	17.25
Zeta Potential (mV)	-14.733 ± 3.60	-15.50 ± 5.3	-14.43 ± 4.20	-16.02 ± 5.42

(2), Initial adsorption/deposition rate on different surfaces

The initial adsorption rate gives us information regarding which functional groups and conditions are most favorable to induce alginate fouling. The initial adsorption/deposition rates of alginate onto different surfaces were summarized in Figure 8. Compared with a similar experiment of the initial adsorption rate of alginate on these SAM surfaces in much lower ionic strength conditions [43], the initial rates in the present conditions are much lower. This can be attributed to the decreased diffusive mass transfer rate for the increased particle sizes of alginate aggregates, due to charge screening destabilization in high ionic strength conditions and cross-linking by cations.

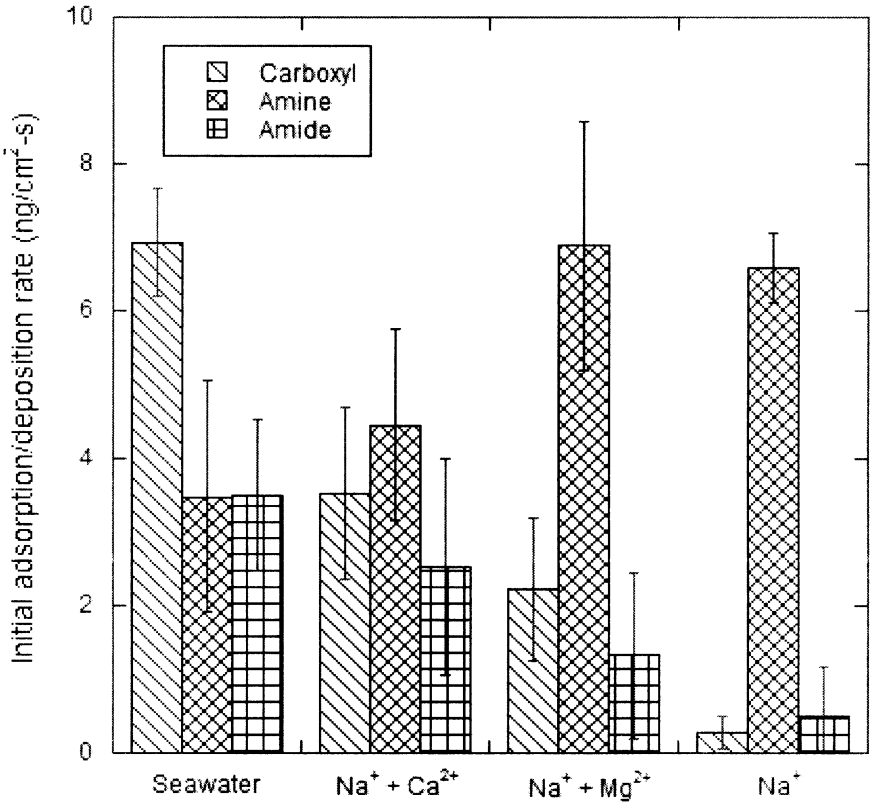

Figure 8 Initial adsorption/deposition rates on different surfaces under different conditions

At the first glance of Figure 8 a very distinct trend of the initial rate for $-NH_2$ group in different solution conditions can be observed compared with those for –COOH and $-CONH_2$. The initial adsorption rate on $-NH_2$ surface decreased in solution conditions with Ca^{2+}, while the presence of divalent ions increased the initial adsorption/deposition rate on –COOH and $-CONH_2$ surfaces. Increased initial rates with the presence of Ca^{2+} is expected, for similar reason stated previously that Ca^{2+} increase the adhesion between alginate molecules thus facilitates the adsorption process. This tendency was also found in other research in low ionic strength conditions

[43]. The different trend on $-NH_2$ surfaces is postulated to be influenced by the electrostatic attraction between alginate molecules and the $-NH_2$ surfaces. In Na^+ and $Na^+ + Mg^{2+}$ solutions, initial adsorption/deposition rate was very high on $-NH_2$ surfaces because alginate molecules are negatively charged while $-NH_2$ surfaces are positively charged, resulting in electrostatic attraction interaction. When there was Ca^{2+} present in the solutions, due to specific interactions between Ca^{2+} and –COOH groups in alginate molecules, the negative charges of alginate are largely neutralized. The reduced charge of alginate led to decreased attraction forces between alginate molecules and the surface, resulted in decreased initial adsorption/deposition rate on $-NH_2$ surfaces in seawater and $Na^+ + Ca^{2+}$ compared with in Na^+ and $Na^+ + Mg^{2+}$.

For –COOH groups it can be observed that the change in ionic composition of the solution had more prominent influence on the initial rate of adsorption/deposition. A steady increase of adsorption rate is shown from solution conditions of Na^+ to seawater. This suggests that specific interactions between –COOH groups, both on the SAM and in alginate, and cations have great influence over the initial contact. Moreover, Ca^{2+} appeared not to be dominant ion in seawater controlling the initial adsorption/deposition rate of alginate on –COOH, as can be seen from the significant different between the adsorption rates in $Na^+ + Ca^{2+}$ and seawater.

This is different from what was observed for the equilibrium adsorption/deposition mass on SAMs.

From the initial adsorption/deposition results, we can see that surface functionality has certain influence on the initial adsorption rate. More exposed –COOH groups will likely accelerate fouling.

4.1.3, Cleaning of adsorbed/deposited mass on different surfaces

The effectiveness of 2% SDS cleaning was represented by the fraction removal of the equilibrium mass on the surfaces. The stage of buffer rinsing after 2% SDS cleaning was modeled and the results were used as the residue mass on the surfaces. The results are averages over two experiments and the error bars represent the range of the data. The cleaning results are summarized in Figure 9.

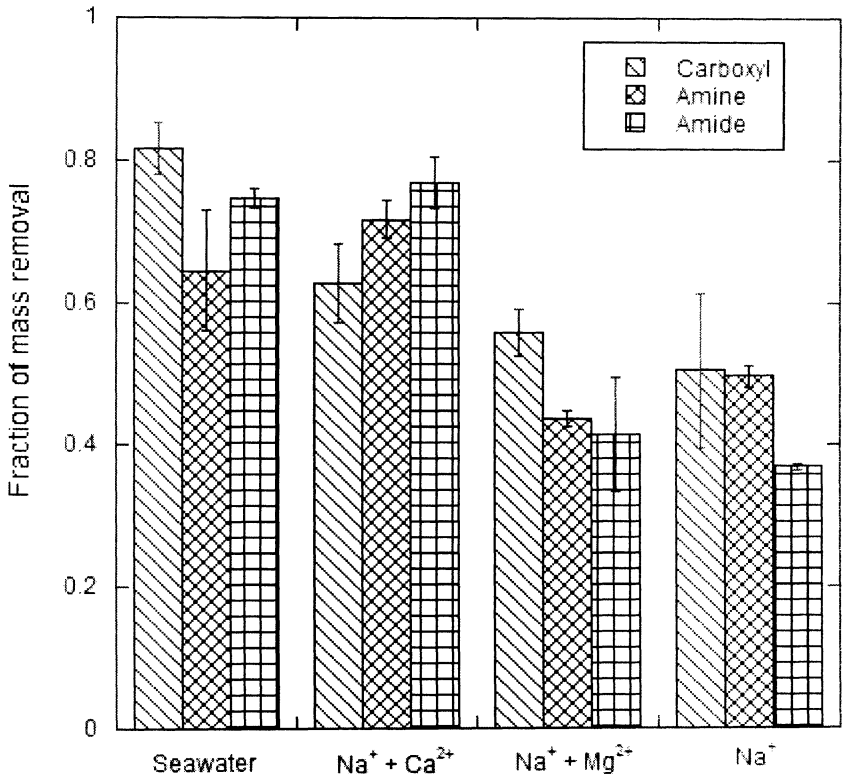

Figure 9 Fractions of mass removal on different surfaces

On different SAM surfaces, $-CONH_2$ had the lowest cleaning efficiency when no divalent cations present, while $-NH_2$ showed relatively low cleaning efficiency in seawater. The low cleaning efficiency for $-CONH_2$ in Na^+ and $Na^+ + Mg^{2+}$ can be attributed to the hydrogen bonding between the carboxylic groups of alginate and the $-CONH_2$ on the surface. As Ca^{2+} was present, bridging between Ca^{2+} and –COOH on alginate resulted in less hydrogen bonding and increased cleaning effectiveness. The low removal efficiency of $-NH_2$ is speculated to be caused by hydrogen bonding.

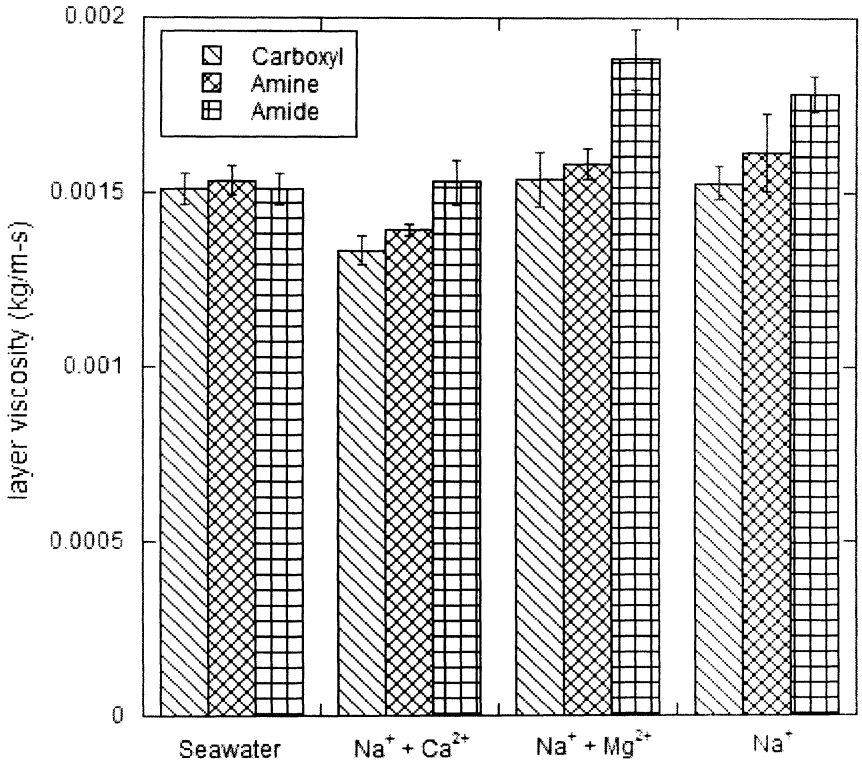

Figure 10 Viscosity of the absorbed/deposited layer on different surfaces

It is interesting to notice that the effectiveness of SDS cleaning of the absorbed/deposited mass, to a certain degree, correlates with the viscosity of the absorbed/deposited layers (Figure 10), especially for $-CONH_2$ surfaces. Intuitively, layers that are more viscous tend to be more difficult to be cleaned off. The decreased layer viscosity in seawater and $Na^+ + Ca^{2+}$ solution conditions are possibly due to the lower packing density for particles of larger sizes [17].

4.2, Filtration Experiment Results

Lab scale filtration experiments with four commercial RO membranes, namely SWC-5, SN, SHF and TM820C, were carried out in order to see if the trend observed in the QCM-D experiment could be applied to more practical conditions. The membranes were characterized of their hydrophobicity, surface roughness and surface chemistry. Fouling experiments in a cross-flow system were then conducted and the flux curves of the membranes were compared in accordance with their surface characteristics.

4.2.1, Membrane characterizations

(1) Membrane surface hydrophobicity and surface roughness

Membrane surface hydrophobicity and surface roughness were measured by contact angle analysis and Atomic Force Microscopy (AFM) respectively. Contact angles of deionized water and seawater on membrane surfaces were measured, and AFM measurements of surface roughness were done for membranes both in air and in seawater. The results are summarized in Figure 11.

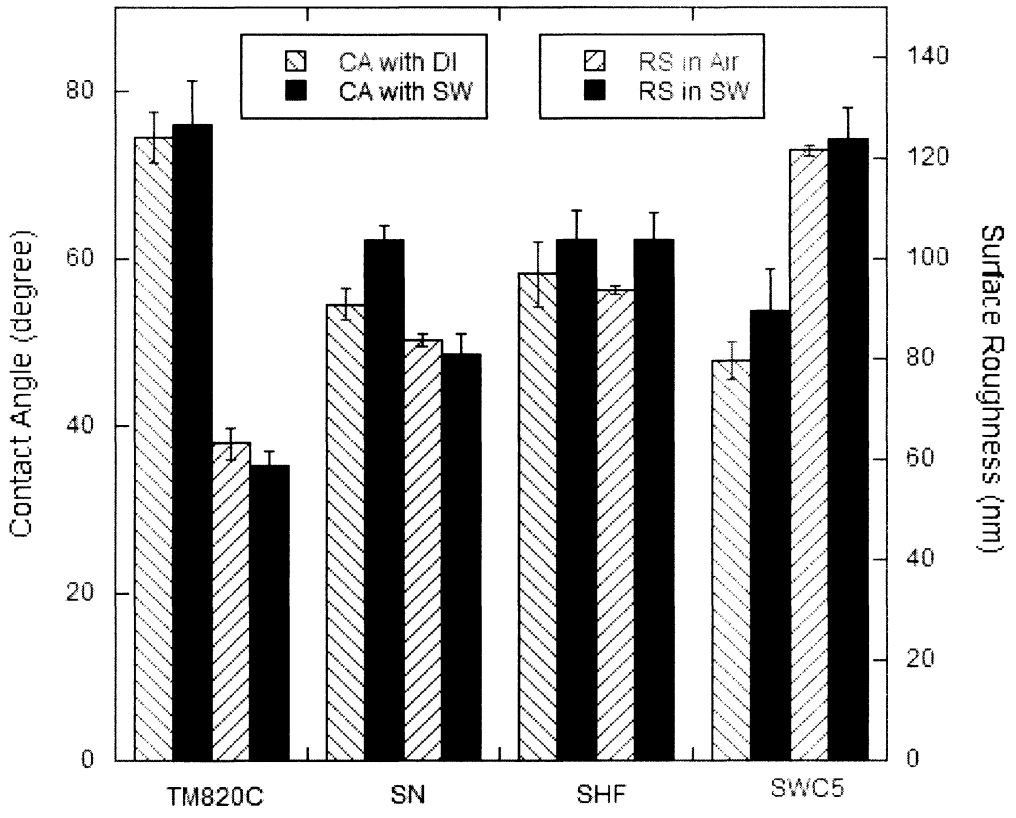

Figure 11 Contact angle and surface roughness characterization of the commercial membranes (CA: Contact Angles; RS: roughness)

For surface hydrophobicity we can see that there are certain degrees of difference in contact angles among the four membranes. TM820C membrane exhibited the highest contact angle with both DI water and seawater, while SWC5 membrane was the most hydrophilic ones shown by their low contact angles. Contact angle measured with seawater slightly increased for all membranes compared with DI water, but did not disrupt the order of hydrophobicity for the four membranes. The increase in contact angles with liquid probes of higher TDS solution was also observed in other research, and was attributed to the enhanced non-polar character of the

membrane surface caused by the double layer compression at solid-liquid interface due to higher ionic strength, as well as the reduced polymer wettability by higher salinity solutions [45, 46].

Surfae roughness for all membranes showed obvious differences, following the order of SWC5 > SHF > SN > TM820C. SWC5 showed the highest roughness of over 120 nm, while the most smooth membrane TM820C had a roughness less than 65 nm. The influence of fluid medium (air versus seawater) on roughness for all the membranes were somewhat ambigious. Previous researches had shown both increased and decreased surface roughness at high salinity conditions [45]. Osmostic pressure driven membrane swelling could cause increased surface roughness. At the same time, charge screening of charged functional groups could reduce the electrostatic repulsive force between polymer backbones, resulting in a more compact, smooth surface [45]. Nevertheless measurement in air or seawater did not change the order of roughness for the four membranes tested, and for the purpose of this study the exact behaviors of membranes when switched from air to seawater are not of primary concern.

(2), FTIR spectrum of membrane chemical compositions

FTIR spectra for the four membranes are shown in Figure 12. Figure 12 (a) shows the spectra over 500 to 4000 cm^{-1} wave number. The spectrums for the four membranes are very similar and show characteristics for typical polyamide membrane with polysulfone backlayer[31]. Figure 12 (b) zooms in to the wave number range of 1000 to 1800 cm^{-1}. The penetration depths of ATR-FTIR are different with respect to wave numbers. At lower waver numbers (500 - 2000 cm^{-1}), ATR-FTIR could penetrate over 300 nm and pick up both spectra of polyamide and polysulfone. So the similarity of spectrums showed in Figure 12 (b) proves that the membranes selected in this experiment are of similar basic chemical compositions and structure. Some signature peaks in the spectrums include: aromatic in-plane ring bend stretching vibration at around 1587, 1504, 1488 cm^{-1} [32]; symmetric deformation vibration of $C(CH_3)_2$ exhibits weak peaks around 1365 to 1385 cm^{-1} [32]; asymmetric and symmetric SO_2 stretching vibration in the polysulfone layer are picked up in 1280 to 1350 and 1145 to 1180 cm^{-1} respectively [32]; and the C-O-C asymmetric stretching vibrations in the polysulfone layer are picked up very strongly at peak around 1245 cm^{-1}[32]. The peaks associated with the –amide functionality are relatively weak in the spectrums. The small peaks at 1541, 1609 and 1663 cm^{-1} are assigned to

amide II band, aromatic amide and amide I band respectively [32], and they signify the presence of polyamide.

At higher wave numbers (over 3000 cm^{-1}), ATR-FTIR are more surface-sensitive, with penetration depth < 200nm. The broad band around 3300 cm^{-1} is likely a mixture of the stretch vibration of N-H and carboxyl groups in the polyamide layer [32], or surface moisture.

Observing from Figure 12 (b), we can see that the absorbance intensities for different membranes at wave numbers signifying –amide functional groups exhibit quite obvious differences, while for the nearby peaks or the baseline the absorbance does not show much difference. This phenomena may suggest that the abundance of –amide groups on different membranes are different. However, FTIR are normally used or qualitative analysis and are not suitable for quantitative analysis without internal standard. In addition FTIR detections for desired functionalities are not surface-sensitive enough for the purpose of surface functionality characterization. So other characterization methods are needed in order to compare the surface functional group compositions in these commercial membranes.

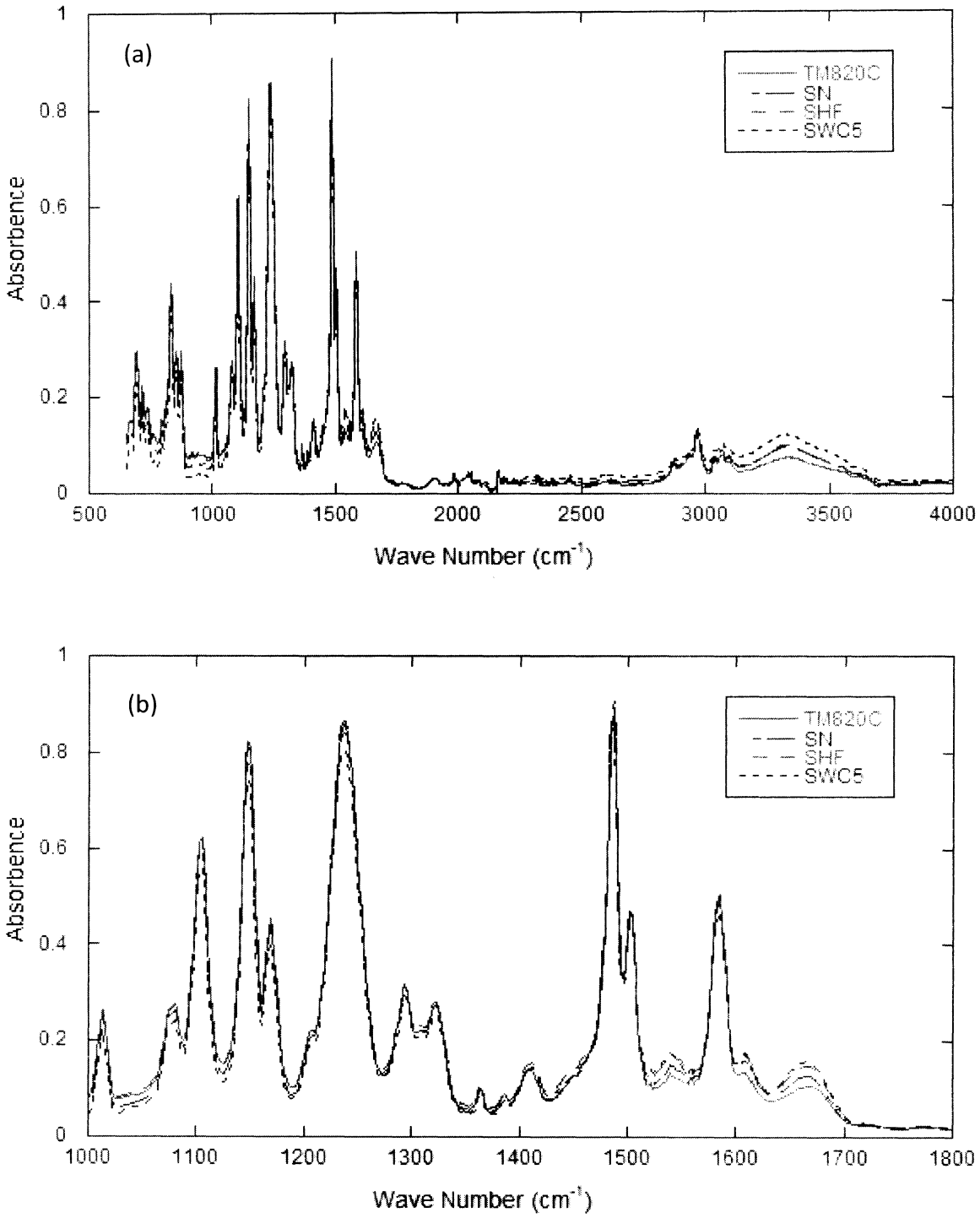

Figure 12 FTIR spectrums of the RO membranes (a) over 500 to 4000 cm^{-1} (b) over 1000 to 1800 cm^{-1}

(3), XPS characterization of surface elemental composition and estimation of functional groups

The XPS characterizations of the elemental composition of the membrane surfaces are summarized in Table 6. XPS is a highly surface sensitive technique that is able to measure the elemental composition within less than 5 nm from the top surface, which gives us confidence in utilizing this information to obtain membrane surface functionality information.

Table 6 Elemental composition of membrane active layer by XPS analysis

	C (%)	O (%)	N (%)	O/N ratio
TM820C	69.7	17.3	13.0	1.331
SN	72.6	14.7	12.7	1.157
SHF	74.5	13.8	11.8	1.170
SWC5	75.0	12.7	12.3	1.033

As was covered in the literature review section, the most commonly used recipe for formation of fully aromatic polyamide membrane is by interfacial polymerization of benzenediamine and trimesoyl chloride. Our FTIR spectra and XPS data largely support that the surface active layer of the membranes are formed by this method [31]. From the scheme (Figure 1) we can see that the polyamide with different levels of crosslinking would exhibit different composition. The theoretical composition for fully cross-

linked polyamide is C_6H_4ON, while that for fully linear polyamide is $C_{15}H_{10}O_4N_2$. The theoretical elemental abundance for fully cross-linked polyamide is 12.5% Nitrogen, 12.5% Oxygen and 75% Carbon, and for fully linear polyamide is 9.5% Nitrogen, 19.1% Oxygen and 71.4% Carbon. The XPS results for the four membranes are generally around this range. Difference in composition, however, can also be observed. TM820C membrane has a high O/N ratio, indicating it is less cross-linked compared with the others.

In order to assess the abundance of functional group at the membrane surfaces, an estimation was given to relate the degree of cross-linking to functional groups. Several assumptions are made for this estimation: first of all, the membrane surface active layers are all interfacially polymerized polyamide; secondly, there are no surface coating present above the active layer; and thirdly, the degree of polymerization for the polyamides on different membranes are similar, and that XPS measures approximately the same volume of samples every time.

For a polyamide macromolecule the degree of cross-linking is closely related to the O/N ratio. As we already summarized in the previous paragraph, for a fully cross-linked polyamide the O/N ratio should be 1,

while for a fully linear polyamide the O/N ratio is 2. O/N ratio could reflect how much of the –COOH and $–NH_2$ groups are reacted to form –CONH– groups. The higher the O/N the more –COOH, $–NH_2$ and less –CONH– are presented on the surface. This serves an indirect way for us to compare surface functional groups.

As summarized in Table 6, the O/N ratio for different membranes can be categorized into three groups. The first group has high O/N ratio above 1.3 (TM820C, 1.331), and the second group has relatively lower O/N ratio above 1.1 (SHF, 1.170 and SN, 1.157), while the third group has low O/N ratio above 1.0 (SWC5, 1.033). So it is expected that more –COOH and $–NH_2$ are present on the surface of TM820C membrane, while more cross-linked –NHCO– on SWC5 membranes. This trend also coincides with the difference in peak height for amide bands in the FTIR spectrums.

Comparing the estimated degree of cross-linking with the surface physical properties, we can see that cross-linking correlates with the hydrophobicity of the membranes, the more cross-linking of the surface, the lower contact angle. From the contact angle analysis of the SAMs we know that for the major functional groups on polyamide surfaces, $–NH_2$ is the most hydrophobic one and –COOH and $–CONH_2$ are all very hydrophilic. So it is

reasonable that the less cross-linked surfaces will have more $-NH_2$ exposed thus causing the surface to be more hydrophobic. Unexpectedly, a reverse trend is observed for the correlation between surface roughness and cross-linking. Study has shown that the synthesis chemistry of monomers has influences on polyamide surface roughness, and it is believed that increased degree of cross-linking will reduce the surface roughness of polyamide [47]. However, it is also found that the meta-positioned polyamides (i.e., polyamide synthesized with 1,3-benzenediamine) have rougher surface than the para-positioned polyamides (i.e., polyamide synthesized with 1,4-benzenediamine) [47]. It is likely that the surface roughness of the commercial membranes in this experiment is influences by this factor.

4.2.2, Fouling experiment

(1), Comparison of flux decline

Fouling experiments are carried out by the protocol and conditions described in the previous section. The permeate flux is normalized by the initial flux before fouling ensued and plotted with accordance of normalized time (Figure 13).

We can see from the flux curves that all the membranes exhibited similar flux decline when the flux reached quasi-steady state. This is likely

due to the fact that the fouling experiment was run under accelerated fouling conditions with very high alginate concentration (100 mg/L). The high foulant availability and mass transfer rate masked the potential difference in flux decline for different membranes.

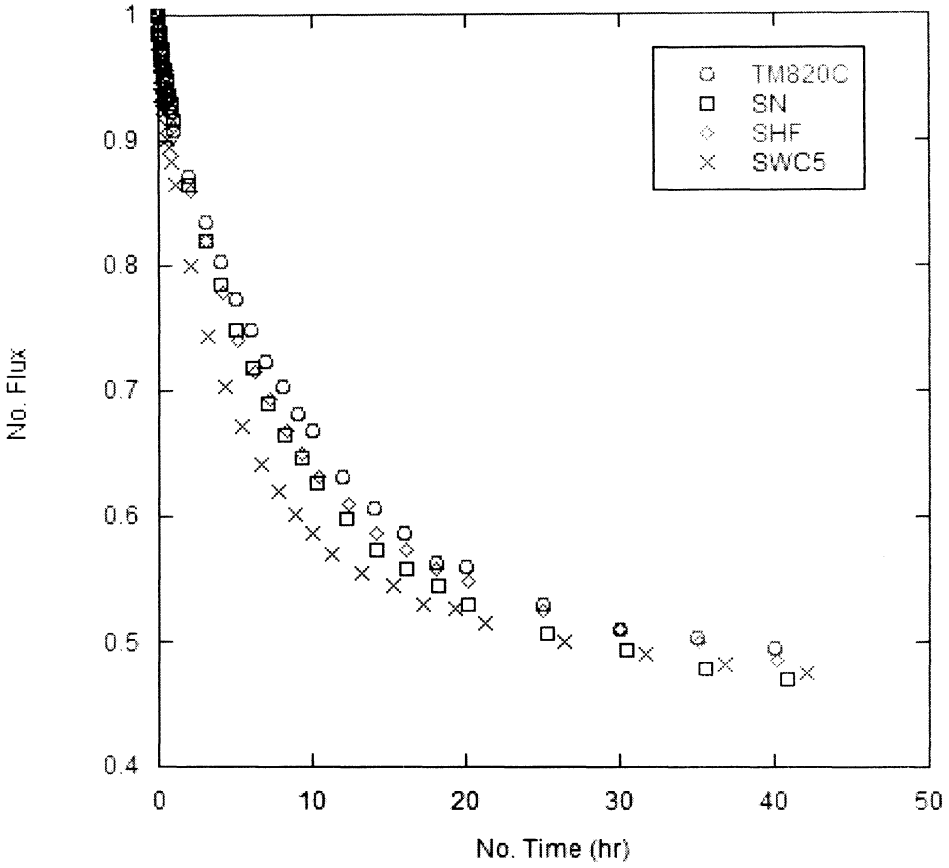

Figure 13 Flux curve of different membranes during fouling

However, difference in the degree of flux decline can still be observed clearly for different membranes. As it is shown in Figure 13, flux decline from 1 hr to 20 hr exhibited clear difference of SWC5 > SHF ≥ SN > TM820C. This trend in some degree correlates with the surface roughness

properties of the membranes. Many studies have indicated that surface roughness had great influence on the rate of fouling for RO and NF membranes, and that more smooth membranes are generally less prone to fouling. The observed difference in flux decline generally agrees with this theory.

Figure 14 is a close-up figure focusing on the flux decline behavior within one hour of the fouling experiment. We can see from the figure the rate of initial flux decline had a different trend of SWC5 > TM820C > SN > SHF, compared with what was observed during 1 to 20 hr. This trend, however, bares no correlation with the characteristics of surface roughness of the membrane. The rate of flux decline for TM820C was much faster at initial stage compared with after 1 hr. This is likely an indication of the influence of surface chemistry and surface hydrophobicity. TM820C membrane has the highest O/N ratio and is likely less cross-linked. So the surface exerted more hydrophobic characteristics and was more likely to be fouled. Also the uncross-linked –COOH groups would likely enhance the attachment and adsorption of alginate, as is showed in the initial rate of adsorption/deposition on SAMs in the QCM-D experiment. However surface chemistry only seemed to have an observable effect on the smoothest

membrane, while SWC5 with the most roughness remain the fastest fouling rate throughout the experiment.

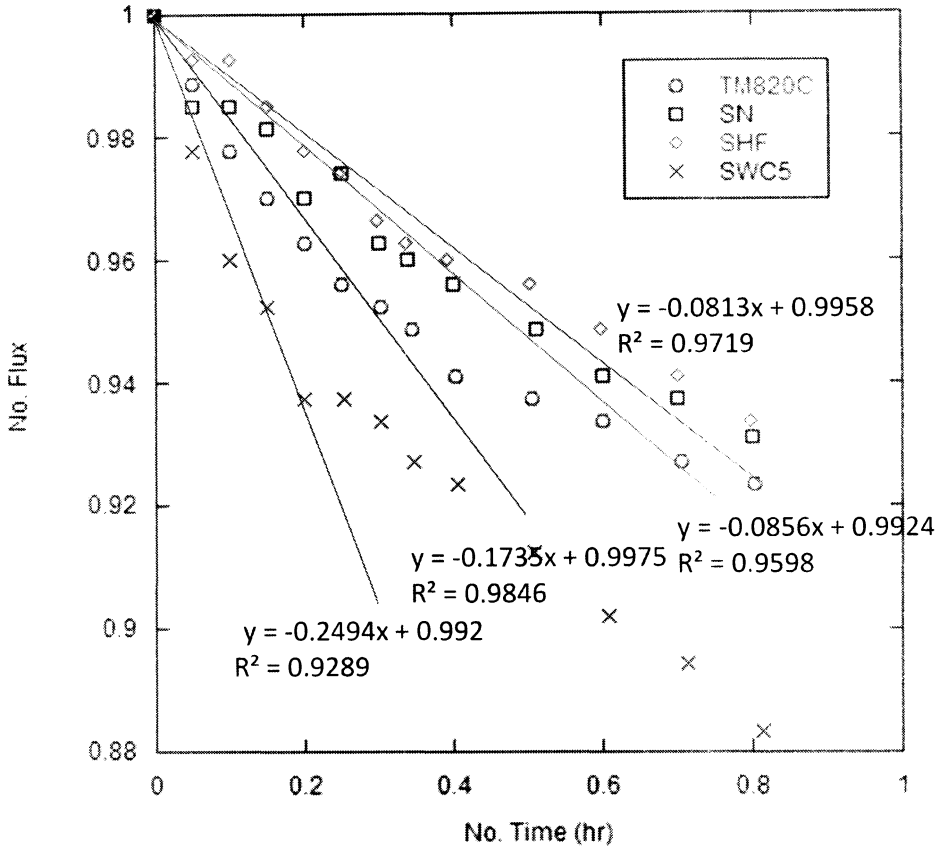

Figure 14 Initial flux decline within one hour for different membranes

This result indicates that during actual membrane filtration, fouling is still more closely related with the surface roughness of the membranes. Chemical functionalities and surface hydrophobicity only exert its influence during the early stage of fouling. This is intuitive to accept as functional groups would affect the initial contact between foulant and membrane

surface, and would be less influential as the fouling layer builds up and the functional groups are less exposed.

(2), Comparison of effectiveness of SDS cleaning

Effectiveness of SDS cleaning is represented by the ratio of clean water flux during compaction and after cleaning (Table 7). Since

$$\mathbf{F = \frac{P_{apply}}{R_{obser}}} \quad \textbf{(8)}$$

Where F is the permeate flux

P_{apply} is the applied pressure

R_{obser} is the observed resistance of the membrane

We can see that the ratio of clean water flux before fouling and after cleaning is essentially the ratio of the observed resistance of the membrane after cleaning to the intrinsic resistance of the membrane. The higher the ratio indicates more irreversible fouling took place on the surface that increased the resistance of the membrane.

Table 7 Ratio of resistance after fouling/cleaning to intrinsic membrane resistance

	TM820C	**SN**	**SHF**	**SWC5**
R'/R_0	1.08	1.05	1.10	1.05

From the data summary we can see that SDS cleaning generally showed fairly good cleaning effectiveness on all four membranes. However, only limited difference between the ratios of resistances among the four membranes were observed. It is insufficient to draw conclusions confidently regarding the influences of membrane surface properties to SDS cleaning of fouled mass. This lack of difference in cleaning effect can also be attributed to the high concentration of alginate used in the filtration/fouling experiment. It has been seen that at high concentration with presence of Ca^{2+} the alginate fouling on the membranes would form highly-gelled layers that could easily be peeled of entirely. It is possible that the high alginate-alginate attraction under the experimental condition overweighs the alginate-surface interactions, causing the adsorbed layer to be more easily to clean off and showed less difference with different membrane surface properties.

5, Conclusions

This thesis focused on studying the influence of membrane surface functionality on alginate fouling in seawater desalination conditions. The research consists of two parts. In the first part experiments were carried out in QCM-D systems to study the adsorption/deposition behaviors of alginate onto different functional-group-terminated SAM surfaces, in solution conditions of different ionic compositions. The results show that solution condition is most crucial in governing alginate fouling of RO membranes; the influence of Ca^{2+} is dominant in affecting the adsorption/deposition amount. Surface functionality does not have significant influence on the total alginate adsorption in seawater, but –COOH does accelerate the initial rate of alginate adsorption under seawater condition. SDS cleaning shows that the amount of residual alginate was highest on $-NH_2$ surfaces under seawater conditions.

The second part of the research involves lab-scale filtration experiments with commercial membranes. Both the surface physical and chemical characteristics of the membrane are analyzed and compared with the flux decline by alginate fouling. The results show that fouling was more closely related with surface roughness than other surface properties. While

hints of influence of surface chemical composition could be seen at the initial stage of membrane fouling, the overall impact of surface functionality on fouling is small. This suggests that in RO seawater desalination, surface functionality is not as important a property as surface roughness for short term alginate fouling.

References

1. U.S. Census Buraeu, World Population Summary, *www.census.gov/ips/www/idb/worldpopinfo.php*. 2011.

2. Kah Peng Lee, T.C.A., Davide mattia, A review of reverse osmosis membrane materials for desalination - Development to date and future potential. Journal of Membrane Science, 2011. **370**: p. 1-22.

3. Lauren F. Greenlee, D.F.L., Benny D. Freeman, Benoit Marrot, Philippe Moulin, Reverse osmosis desalination: Water sources, technology, and today's challenges. Water Research, 2009. **43**: p. 2317-2348.

4. C. Fritzmann, J.L., T.Wintgens, T.Melin, State-of-the-art of reverse osmosis desalination. Desalination, 2007. **216**: p. 1-76.

5. Van der Bruggen, B., Vandecasteele, C., Distillation vs. membrane filtration: overview of process evolutions in seawater desalination. Desalination, 2002. **143**: p. 207-218.

6. Loeb, S., Sourirajan, S., , Seawater dimineraliaztion by mean of an osmotic membrane. Advances in Chemistry, 1963. **38**: p. 117-132.

7. D.E. Potts, R.C.A., S.S.Wang, A critical review of fouling of reverse osmosis membrane. Desalination, 1981. **36**: p. 236-264.

8. Sangho Lee, J.K., Chung-Hak Lee, Analysis of $CaSO_4$ scale formation mechanism in various nanofiltration modules. Journal of Membrane Science, 1999. **163**: p. 63-74.

9. Khalid Burashid, A.R.H., Seawater RO plant operation and maintence experience: Addur desalination plant operation assesement. Desalination, 2004. **165**: p. 11-22.

10. Elftheria Neofotistou, K.D.D., Use of antiscalants for mitigation of silica fouling and deposition: fundamentals and application in desalination systems. Desalination, 2004. **167**: p. 257-272.

11. M.Al-Ahmad, F.A.A.A., A. Mutiri, A. Ubaisy, Biofouling in RO membrane systems Part 1: Fundamentals and control. Desalination, 2000. **132**: p. 173-179.

12. Dooil Kim, S.J., Jinsik Sohn, Hyungsoo Kim, Seockheon Lee, Biocide application for controlling biofouling of SWRO membranes - an overview. Desalination, 2009. **238**: p. 43-52.

13. Nobuya Fujiwara, H.M., Elimination of biological fouling in seawater reverse osmosis desalination plants. Desalination, 2008. **227**: p. 295-305.

14. Abdul Ghani I. Dalvi, R.A.-R., Mohammad A. Javeed, Studies on organic foulants in the seawater feed of reverse osmosis plants of SWCC. Desalination, 2000. **132**: p. 217-232.

15. Sangho Lee, J.-S.C., Chung-Hak Lee, Behaviors of dissolved organic matter in membrane desalination. Desalination, 2009. **238**: p. 109-116.

16. Huanjuan Mo, K.G.T., How Yong Ng, Fouling of reverse osmosis membrane by protein (BSA): effects of pH, calcium, magnesium, ionic strength and temperature. Journal of Membrane Science, 2008. **315**: p. 28-35.

17. Karina Listiarini, L.T., Darren D. Sun, James O. Leckie, Systematic study on calcium-alginate interaction in a hybrid coagulation-nanofiltration system. Journal of Membrane Science, 2011. **370**: p. 109-115.

18. K.S. Katsoufidou, D.D.S., S.G. Yiantsios, A.J. Karabelas, UF membrane fouling by mixture of humic acid and sodium alginate: Fouling mechanisms and reversibility. Desalination, 2010. **264**: p. 220-227.

19. Baoxia Mi, M.E., Organic fouling of forward osmosis membranes: Fouling reversibility and cleaning without chemical reagents. Journal of Membrane Science, 2010. **348**: p. 337-345.

20. Alison E. Contreras, A.K., Qilin Li, Combined fouling of nanofiltration membranes: Mechanisms and effect of organic matter. Journal of Membrane Science, 2009. **327**: p. 87-95.

21. Sungyun Lee, S.K., Jaeweon Cho, Eric M.V. Hoek, Natural organic matter fouling due to foulant-membrane physicochemical interactions. Desalination, 2007. **202**: p. 377-384.

22. Juhee Yang, S.L., Youngbeom Yu, Jihun Kun, Seungkwan Hong, Seungyoon Lee, Kyungsok Min, Role of Foulant-Membrane Interactions in Organic Fouling of RO Membranes with Respect to Membrane Properties. Separation Science and Technology, 2010. **45**: p. 948-955.

23. Meng Yao, K.Z., Li Cui, Characterization of protein-polysaccharide ratios on membrane fouling. Desalination, 2010. **259**: p. 11-16.

24. Mika Manttari, L.P., Jutta Nuortila-Jokinen, Marianne Nystrom, Fouling effects of polysaccharides and humic acid in nanofiltration. Journal of Membrane Science, 2000. **165**: p. 1-17.

25. Colin Hobbs, S.H., James Taylor, Effect of surface roughness on fouling of RO and NF membrane during filtratino of a high organic surficial groundwater. Journal of Water Supply: Research and Technology, 2006. **55**: p. 7-8.

26. Catherine Jucker, M.M.C., Adsorption of aquatic humic substances on hydrophobic ultrafiltration membranes. Journal of Membrane Science, 1994. **97**: p. 37-52.

27. Menachem Elimelech, X.Z., Amy E. Childress, Seungkwan Hong, Role of membrane surface morphology in colloidal fouling of cellulose acetate and composite aromatic polyamide reverse osmosis membranes. Journal of Membrane Science, 1997. **127**: p. 101-109.

28. Eric M.V. Hoek, S.B., Menachem Elimelech, Effect of Membrane Surface Roughness on Colloid-Membrane DLVO Interactions. Langmuir, 2003. **19**: p. 4836-4847.

29. Qilin Li, Z.X., Ingo Pinnau, Fouling of reverse osmosis membranes by biopolymers in wastewater secondary effluent: Role of membrane surface properties and initial permeate flux. Journal of Membrane Science, 2007. **290**: p. 173-181.

30. Xinyu Wei, Z.W., Zhe Zhang, Jixiao Wang, Shichang Wang, Surface modification of commercial aromatic polyamide reverse osmosis

membrane by graft polymerization of 3-allyl-5,5-dimethylhydantoin. Journal of Membrane Science, 2010. **351**: p. 222-233.

31. Chuyang Y. Tang, Y.-N.K., James O. Leckie, Probing the nano- and micro-scales of reverse osmosis membranes - A comprehensive characterization of physiochemical properties of uncoated and coated membranes by XPS, TEM, ATR-FTIR, and streaming potential measurements. Journal of Membrane Science, 2007. **287**: p. 146-156.

32. Chuyang Y. Tang, Y.-N.K., James O. Leckie, Effect of membrane chemistry and coating layer on physiochemical properties of thin film composite polyamide RO and NF membranes I. FTIR and XPS characterization of polyamide and coating layer chemistry. Desalination, 2009. **242**: p. 149-167.

33. Chuyang Y. Tang, Y.-N.K., James O. Leckie, Effect of membrane chemistry and coating layer on phsiochemical properties of thin film composite polyamide RO and NF membranes II. Membrane physiochemical properties and their dependence on polyamide and coating layers. Desalination, 2009. **242**: p. 168-182.

34. Chia-Chi Ho, B.N.R.P., Brian Kiessling, Carlos C. Co, Effects of membrane surface chemistry on fouling investigated using self-assembled monolayers. Journal of Membrane Science, 2011. **366**: p. 342-348.

35. Gwen Lawrie, I.K., Barry Drew, Adriene Chandler-Temple, Llewellyn Rintoul, Peter Fredericks, Lisbeth Grondahl, Interactions between alginate and chitosan biopolymers characterized using FTIR and XPS. Biomacromolecules, 2007. **8**: p. 2533-2541.

36. Toshio Yoshimura, M.M., Rumiko Fujioka, Alginate-based superabsorbent hydrogels composed of carboxylic acid-amine interaction: preparation and characterization e-Polymer, 2009. **80**: p. 1-8.

37. Sean X. Liu, J.-T.K., Application of Kevin-Voigt Model in Quantifying Whey Protein Adsorption on Polyethersulfone Using QCM-D. Journal of the Association for Laboratory Automation, 2009. **14**(4): p. 213-220.

38. Hook, F., Development of a novel QCM technique for protein adsorption studies. PhD thesis, 1997.

39. Marc Meyers, K.C., Mechanical Behavior of Materials. Second Edition ed. 2009: Cambridge University Press.

40. M.V. Voinova, M.R., M. Jonson, B. Kasemo, Viscoelastic Acoustic Response of Layered Polymer Films at Fluid-Solid Interfaces: Continuum Machanics Approach. Physica Scripta, 1999. **59**: p. 391-396.

41. Xue Jin, X.H., Eric M.V. Hoek, Role of Specific Ion Interactions in Seawater RO Membrane Fouling by Alginic Acid - Supporting Information. Environmental Science & Technology, 2009. **43**: p. 3580-3587.

42. QCM-D viscosity measurement. Q-TOOLS DATA ANALYSIS, Q-SENSE AB 2007.

43. Alison E. Contreras, Z.S., Jing Miao, Roni Kasher, Qilin Li, Studying the impact of membrane surface chemistry on adsorption and cleaning of organic foulants using QCM-D. Environmental Science & Technology, 2011. **45**: p. 6309-6315.

44. Kohn, R., Ion binding on polyuronates - alginate and pectin. Seventh International Symposium on Carbohydrate Chemistry, Bratislava, Czechoslovakia, 1974(5-9 August).

45. Juhee Yang, S.L., Eunsu Lee, Joohee Lee, Seungkwan Hong, Effect of solution chemistry on the surface property of reverse osmosis membranes under seawater conditions. Desalination, 2009. **247**: p. 148-161.

46. Gillian B. Kaggwa, S.F., Le Huynh, John Ralston, Kristen Bremmell, Morphology of Absrobed Polymers and Solid Surface Wettability. Langmuir, 2005. **21**: p. 4695-4704.

47. Seung-Yeop Kwak, S.G.J., Young Seo Yoon, Dae Woo Ihm, Details of Surface Features in Aromatic Polyamide Reverse Osmosis Membranes Characterized by Scanning Electron and Atomic Force Microscopy. Journal of Polymer Science Part B-Polymer Physics, 1999. **37**: p. 1429-1440.